The Effect of Metal-Support Interactions on Formaldehyde Oxidation and By-Product Selectivities in TiO2 Supported Metal Catalysts (Co, Cr, Mo, and Ag)

Rached Ousji, Zouhaier Ksibi, Abdelhamid Ghorbel, Céline Fontaine

The effect of metal-support interactions on formaldehyde oxidation and by-product selectivities in TiO_2 supported metal catalysts (Co, Cr, Mo, and Ag).

Rached Ousji[1]. Zouhaier Ksibi[1]. Abdelhamid Ghorbel[1]. Céline Fontaine[2]

[1]*University of Tunis El Manar, Faculty of Sciences of Tunis, Laboratory of Materials Chemistry and Catalysis, Tunis, Tunisia*

[2]*University of Poitiers, Institute of Chemistry of Poitiers: Materials and Natural Resources (IC2MP), France*

Abstract

One of the most significant indoor air pollutants is formaldehyde, and long-term exposure to HCHO may cause health problems. Catalytic oxidation at room temperature is an effective technology for removing HCHO indoors. In this paper, a simple sol-gel synthesis method was proposed for the preparation of TiO_2 support, and a series of 5%M (Co, Cr, Mo, and Ag) catalysts were prepared by impregnation process. The materials were characterized by XRD, TEM, FT-IR, BET, and H_2 -TPR. The catalytic activities and the oxidation reaction of HCHO were investigated by an analytical system equipped with an infrared analyser (MKS multigas 2030) to analysis the different products. The results showed that the M/TiO_2 catalysts obtained have TiO_2 anatase phase diffraction peaks as well as a high surface area and porosity. The samples physicochemical, catalytic properties, and by-product selectivity's differ depending on the metal impregnated. The Ag/TiO_2 catalyst was effective for the removal of formaldehyde gas at 95 °C, resulting in the selective production of carbon dioxide and water. The Co/TiO_2 demonstrated complete conversion of HCHO at 244 °C and improved CO_2 selectivity. The TEM images for the Ag/TiO_2 catalyst showed that the silver particles were identified and very well dispersed on the support. Finally, these results might help in the development of high-performance catalysts activities at ambient temperature.

Keywords: formaldehyde, TiO_2, Catalytic oxidation, Sol-Gel, Supported metal catalysts, selectivities, CO_2, temperature

Introduction

Indoor air pollution has become a growing concern in recent years, as people spend a significant amount of time inside buildings and structures, where the concentration of toxic substances such as volatile organic compounds (VOCs) often higher than outdoors [1, 2]. Various toxic substances (VOCs) have been introduced into the indoor environment, such as formaldehyde, benzene, toluene, and so on [3]. Formaldehyde (HCHO) is the primary indoor pollutant emitted by commonly used building and decorative materials and has been linked to various health issues, including cancer [4]. Although various technologies have been developed to reduce the concentration of formaldehyde in indoor air, such as physical adsorption [6, 7], photocatalytic [8, 9], and catalytic oxidation. However, due to its limited adsorption capacity, the adsorbent has an unstable removal impact [5]. The photocatalyst's action can result in secondary toxicity pollution, such as HCHO [5]. In contrast, catalytic oxidation is an effective and environmentally friendly method for formaldehyde elimination into carbon dioxide and water. Metal oxide and noble-metal catalysts have been used for formaldehyde oxidation, and their catalytic performance is closely related to their morphology, surface area, and crystal structure. At room temperature, noble-metal catalysts have very high catalytic performance for HCHO oxidation; for example, Pt/TiO_2 with a Pt loading of 1% exhibited excellent activity for formaldehyde oxidation [9]. Transition metal materials, on the other hand, have received widespread attention due to their low cost and high catalytic activity. Mn [10, 11], Co [12], and Cr [13] have been shown to have good catalytic activity, and metals such as Ce [14], Sn [15], and Cu [16] can be doped into the catalyst as promoters to improve activity. Titanium oxide has long been of interest to scientists as both a catalyst and support material. Its highly developed surface contains both acid-base sites and exhibits high mechanical and thermal stability, enabling the significant dispersion of active phases and providing it with exceptionally interesting properties for use in heterogeneous catalysis. Various methods have been developed to synthesize TiO_2, including the sol-gel method [17]. This method has great potential for producing various material structures, such as bulk, fibres, sheets, films, and particles, at low temperatures [18]. It enables the creation of materials with high purity and homogeneity, as well as the control of particle size distributions at the nanoscale level. In this study, we used sequential sol-gel and impregnation methods to synthesize titanium oxide and load metals onto it. We investigated the effect of the metal type on the catalytic performance for formaldehyde (HCHO) oxidation and detected by-products using an advanced infrared analyser (MKS multigas 2030). To investigate the physicochemical properties of the synthesized catalysts, we used a combination of X-ray

diffraction (XRD), Transmission Electron Microscopy (TEM), Fourier-transform infrared spectroscopy (FTIR), Brunauer-Emmett-Teller (BET), and hydrogen temperature programmed reduction (H_2-TPR).

Experimental section

Catalyst synthesis

All chemical reagents used were of the highest analytical grade. In our study, titanium oxide was synthesized using the sol-gel method and used as a support. Titanium (IV) isopropoxide (70% from S. Aldrich) was dissolved in absolute ethanol (99.8% from S. Aldrich) and stirred for 30 min. To control the hydrolysis and condensation reaction rates, ethyl acetoacetate was added to the solution in a molar ratio of Eacac (Ethyl acetoacetate): Ti =1. After 30 minutes of stirring, 1.5 mL of a 0.1M aqueous nitric acid solution (65% from S. Aldrich) was added dropwise, corresponding to a molar ratio H_2O: Ti =10. The solution was then stirred until a yellow gel formed. The gel was dried in an autoclave under supercritical ethanol conditions (P = 63 bars; T = 243 °C), crushed, and then calcined under an oxygen flow for 3 hours at 500 °C with a temperature rise of 1 °C/min and a flow rate of 30 mL/min.

In the impregnation method, aqueous precursor solutions of cobalt (II) nitrate hexahydrate, chromium (III) chloride, pure molybdenum powder, and silver nitrate were added to the support material while stirring. The M/TiO_2 catalysts were activated by a reduction treatment under H_2 (30 mL/min) at 300 °C with a ramp of 1°C/min after drying at 100 °C for 12 hours. The impregnated solids were labelled as Co/TiO_2, Cr/TiO_2, Mo/TiO_2, and Ag/TiO_2.

Catalysts characterization

Understanding a catalyst's morphological, textural, and structural properties is critical because these properties have a direct impact on the number and accessibility of active sites, as well as the catalytic activity. In what follows, we will discuss the various techniques we used to characterize our catalysts.

The nitrogen physisorption method is commonly used to measure the specific area and porosity of catalysts produced with an ASAP 2020 Micromeritics analyser. Specifically, the BET method is used to calculate the specific surface area (S_{BET}) from the nitrogen adsorption data, using a P/P_0 ratio between 0.04 to 0.31. The desorption branch of the isotherm is then analysed using the Barret-Joyner-Halenda (BJH) model to calculate the total pore volume (Vp) and average pore size (Dp).

Transmission electron microscopy (TEM) images were obtained using an 80 kV JEOL JEM-1011 microscope to gather additional information about the composition, morphology, and structure of the catalysts. The catalysts were mixed with ethanol and dispersed in an ultrasonic bath. Subsequently, the solutions were placed on a copper plate and dried by evaporating the ethanol before the analysis.

The Perkin Elmer spectrometer was used for Fourier transform infrared spectroscopy (FTIR) to identify the molecular bonds in the samples. The samples were analysed using an IR irradiating source in the frequency range of 400-4000 cm^{-1} [19].

To identify the crystalline phases and chemical composition of the catalysts, X-ray diffraction (XRD) was performed using a PANalytical X'pert PRO MPD diffractometer with a $CuK\alpha^1$ radiation (1.54060 Å) in reflection geometry. The diffractograms were recorded over a range of 10-70°, with a step size of 0.017° and a scan step time of 12 seconds. The crystalline phases were identified by comparing them to ICDD PDF standards. The average crystallite size of the samples (d_{XRD}) (in nm) was calculated using Scherrer's equation:

$$d_{XRD} = 0.9\ \lambda / \beta \cos \theta$$

Where K= 0.9, β is the corrected full width at half maximum (in rad), and θ is the Bragg angle of the diffraction peak (in rad).

The programmed H_2 temperature reduction profiles (H_2-TPR) were performed using a Micromeritics AutoChem 2920 analyser. The TPR technique can be used to characterize supported metals and oxides by determining the hydrogen consumption during metal oxide reduction as a function of temperature. A 5% H_2/Ar gas mixture with a ramp rate of 5 °C/min and a flow rate of 30 mL/min was used to achieve temperatures ranging from 40 to 700 °C.

Catalytic activity measurement

The MKS Multigas 2030 infrared analyser was used to set up the oxidation of volatile organic compounds in the gas phase, enabling continuous analysis of several molecules such as formaldehyde, CO_2, CO, methanol, formic acid, and water with a detection threshold of the order of parts per million (ppm).

The formaldehyde used in the tests was derived from paraformaldehyde, which was dissolved overnight with stirring at 50 °C. To stabilize the mixture, the measured mass of the solid was dissolved in 100 mL of ultrapure water and 1 mL of 0.1 mol L^{-1} sodium hydroxide solution.

The catalytic oxidation of HCHO over the catalysts (50 mg) was tested in a glass flow reactor using a gas mixture comprising of 100 ppm HCHO, 19.5% O_2, 78% N_2, and 2.5% H_2O balanced at a total flow rate of 100 cm^3 min^{-1}, and GHSV of 84,000 h^{-1}.

$$HCHO\ Conversion\ (\%) = \frac{[HCHO]_i - [HCHO]_T}{[HCHO]_i} * 100$$

Where $[HCHO]_i$ denotes the initial concentration and $[HCHO]_T$ denotes the concentration during the reaction.

The apparent selectivity's for carbon dioxide, carbon monoxide, methanol, and formic acid are calculated as follows:

$$(Pi)\ selectivity\ (\%) = \frac{[Pi]}{\sum[Pj]} * 100$$

Where [Pi] is the concentration of the product and [Pj] is the sum of all reaction product concentrations.

The previous selectivity values will allow the yields of these products to be calculated as shown in the equation:

$$(Pi)Yield\ (\%) = HCHO\ Conversion * (Pi)\ selectivity$$

Results and discussion

X-Ray Diffraction analysis

Figure. 1 displays the XRD spectra of sol-gel synthesized TiO_2, Co/TiO_2, Cr/TiO_2, Mo/TiO_2, and Ag/TiO_2 catalysts. The anatase phase of each catalyst exhibits prominent peaks indexed using the standard powder diffraction pattern (JCPDS 01-071-1166) with a tetragonal symmetry structure. The rutile phase is not observed since the support TiO_2 was calcined at 500 °C. The anatase phase is identified by the peaks located at 2θ = 25.44°, 38.0°, 48.3°, 54.43°, and 63.4°, which correspond to the (101), (004), (200), (105), and (204) planes, respectively [20-21]. The absence of distinctive peaks corresponding to silver and cobalt in the diffraction pattern suggests that Ag was highly dispersed on the surface of anatase TiO_2, while cobalt can either be inserted in the interstitial sites of the crystal or substitute Ti ions. Furthermore, the smaller ionic radius of Ti^{4+} ion (0.068 nm) compared to that of Ag^+ ion (0.126 nm) makes it difficult for Ag^+ to replace Ti^{4+} in the crystal lattice [22]. However, the ionic radius of Co^{2+} (0.072 nm) is slightly larger than that of Ti^{4+}, making it possible for Co^{2+} to substitute for Ti^{4+} in the titania

lattice [23]. The XRD patterns of Mo/TiO_2 exhibited two diffraction peaks assigned to the cubic molybdenum metallic at 2θ = 40.50° and 58.65°. In contrast, the Cr/TiO_2 XRD patterns revealed a reduction in the intensity of the TiO_2 anatase characteristic peaks and specific peaks at 2θ = 15.27°, 30.82°, 36.53°, 53.27°, and 64.18° corresponding to the monoclinic crystal system of Chromium Chloride ($CrCl_3$). This result suggests that the reduction temperature of the chromium precursor is insufficient to remove chlorine and chromium, which were poorly incorporated into the TiO_2 structure. The addition of metal increased the anatase peaks, indicating a higher degree of crystallinity, and the increase in crystallinity was strongly influenced by the type of metal present in TiO_2. The increase in crystallinity resulting from the presence of metals could be due to metal ions occupying interstitial sites within the crystal or undergoing surface doping [24].

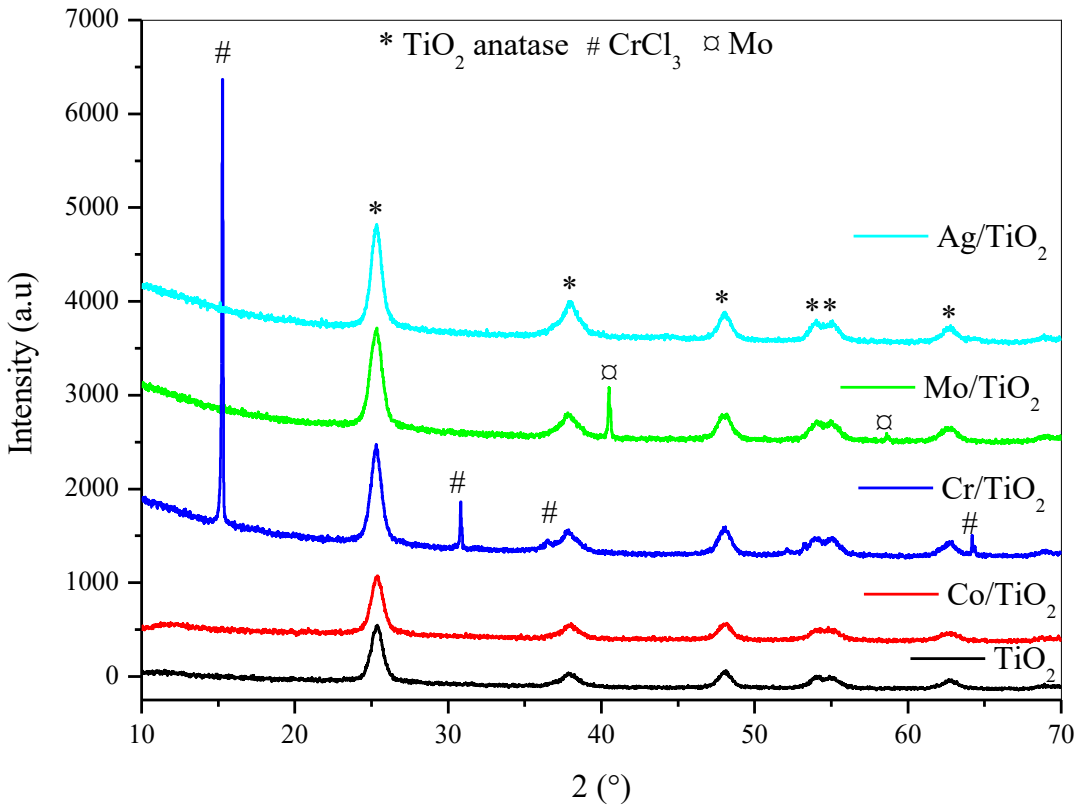

Figure 1. X-ray diffraction of: TiO_2, Co/TiO_2, Cr/TiO_2, Mo/TiO_2 and Ag/TiO_2

Table. 1 shows the crystallite sizes of the synthesized catalysts calculated using the Debye-Sherrer equation. TiO_2 had the smallest crystallite size (12.4 nm), followed by Ag/TiO_2 (14.6

nm), Co/TiO_2 (15.2 nm), Mo/TiO_2 (36.8 nm), and Cr/TiO_2 (61.3 nm). The increased crystal size after metal loading confirmed the higher crystallinity.

Table 1. Material properties of synthesized catalysts

Catalyst	S_{BET} (m^2/g) [a]	Pore volume (cm^3/g) [a]	Average pore diameter(Å) [a]	Crystallite size (nm)[b]
TiO_2	132	0.38	84	12.4
Co/TiO_2	113	0.32	86	15.2
Cr/TiO_2	91	0.24	75	61.3
Mo/TiO_2	118	0.36	85	36.8
Ag/TiO_2	104	0.28	77	14.6

[a] Determined by BET, [b] Determined by XRD

Physisorption measurements

Figure. 2a depicts the N_2 adsorption-desorption isotherms for TiO_2 and various M/TiO_2 samples with 5% metal loading. According to IUPAC classification, all samples resembled the type IV isotherm, a profile characteristic of mesoporous materials [25]. The hysteresis loop associated with isotherms is assigned to the H_2 type, which corresponds to mesoporous textures and ink-bottle shaped pores formed by aggregated spherical particles [26-27]. The BJH pore size distribution of various $M\text{-}TiO_2$ catalysts is depicted in **Fig. 2b**, indicating that all samples have a monomodal size distribution. N_2 adsorption-desorption measurements were used to calculate the BET surface area, pore volume, and average pore diameter of each catalyst (Table 1). Sol-gel synthesized TiO_2 had the highest specific surface area of 132 m^2/g, compared to 118 m^2/g of Mo/TiO_2, 113 m^2/g of Co/TiO_2, 104 m^2/g of Ag/TiO_2, and 91 m^2/g of Cr/TiO_2. The TiO_2 exhibited a much larger surface area, and the decrease of this surface area upon addition metal (Co, Cr, Mo, and Ag) can be explained by the increase of its crystal sizes. TiO_2, Mo/TiO_2, Co/TiO_2, Ag/TiO_2, and Cr/TiO_2 have pore volumes of 0.38, 0.36, 0.32, 0.28, and 0.24 cm^3/g, respectively. The average pore diameter of Co/TiO_2 (86 Å) and Mo/TiO_2 (85 Å) was greater than TiO_2 (84 Å), Ag/TiO_2 (77 Å), and Cr/TiO_2 (75 Å), possibly due to a partial blockage of the pore's support entrances by cobalt and molybdenum species.

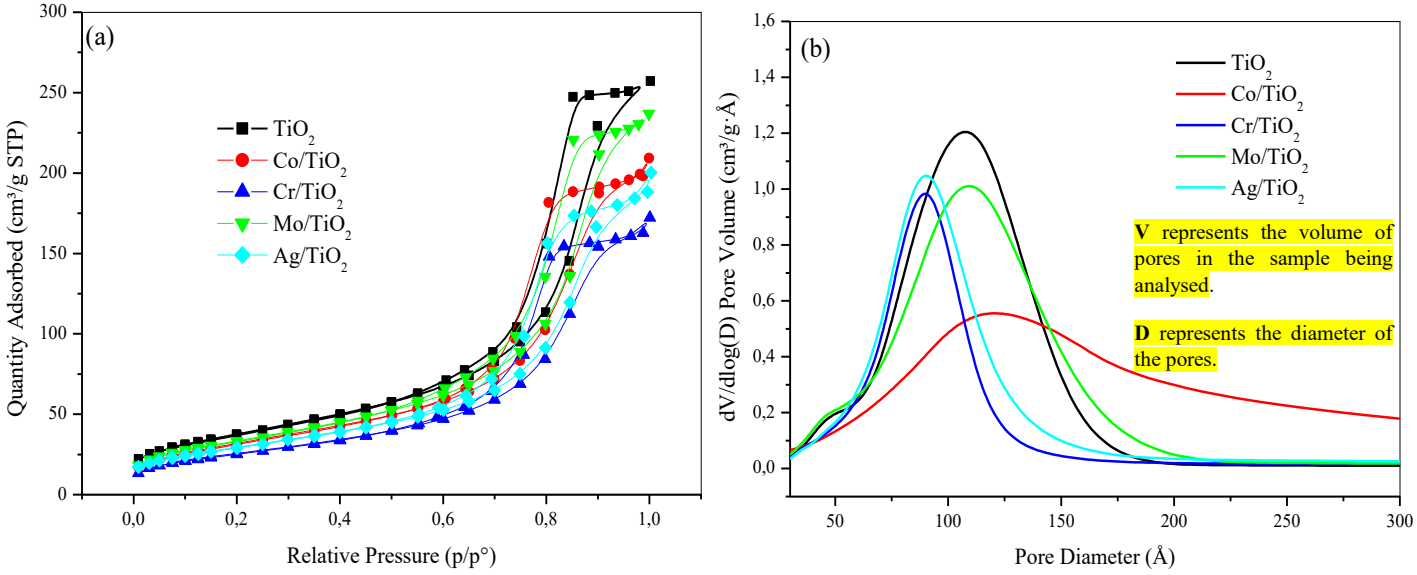

Figure. 2 The curves of nitrogen adsorption-desorption isotherms (a) and the corresponding pore size distribution curves (b) of TiO_2, Co/TiO_2, Cr/TiO_2, Mo/TiO_2 and Ag/TiO_2

Reducibility H_2-TPR analysis

According to prior research, the redox properties of the catalysts, such as low temperature reducibility, surface oxygen distributions, and oxygen mobility in the lattice, have a significant impact on their catalytic behaviour for VOC oxidation [28-29]. Using the H_2-TPR measurement, the hydrogen absorptions could characterize the phenomenon of adsorption and dissociation of hydrogen molecules through chemical combination with active oxygen species at the surface level of metal oxide catalysts [30]. As a result, the information provided by this technique can also be used to evaluate the availability of surface-active oxygen and the abundance of vacant oxygen on metal oxides. **The figure. S1 (from the supporting information)** depicts the TPR-H_2 profiles of the catalysts. The pure TiO_2 profile shows a very broad and low intensity reduction peak at 536 °C, which is related to the sample's low hydrogen consumption. This could be because of resistance to the reducing process. This is due to the surface dehydroxylation of TiO_2 and the reduction of Ti^{4+} to Ti^{3+} [31].

The H_2-TPR profile of the Co/TiO_2 catalyst exhibits two reduction peaks. The first peak, which occurs at 300-400°C, corresponds to the reduction of Co_3O_4 to CoO, resulting in the reduction of Co^{3+} to Co^{2+} metal. The second peak, which occurs at 400-550°C, corresponds to the reduction of CoO to Co, resulting in the reduction of Co^{2+} to Co^0 metal [32]. For Cr/TiO_2 catalysts, a single low-intensity hydrogen consumption peak was observed over the entire temperature range due to the difficulty in reducing the chromium species in the presence of

chlorine. The reduction peak, which appears around 585 °C [33], corresponds to the change in oxidation state from Cr^{3+} to either Cr^{2+} or the metallic state. The TPR profile of Mo/TiO_2 does not exhibit any reduction peaks, indicating that the molybdenum species are in the metallic state in the supported catalyst, which is consistent with the XRD diagram [34]. On the other hand, the TPR profile of Ag/TiO_2 reveals three major peaks with higher H_2 consumption, observed at 85, 125, and 300 °C, respectively. As previously reported [35], the thermal analysis revealed three reduction peaks. The peak observed below 100 °C was attributed to the reduction of chemisorbed oxygen on the catalyst surface. The peak observed at around 100°C was attributed to the reduction of large Ag_2O clusters that had a low concentration or were highly dispersed, which made them undetectable by XRD [36]. Finally, the peak observed around 300 °C was attributed to the reduction of stable and well-dispersed Ag_2O or Ag^+ ions. This clearly demonstrates the presence of strong support-metal interactions between Ag and TiO_2, which enhances the reduction process [36].

FT-IR analysis

The FTIR spectra of (a) TiO_2, (b) Co/TiO_2, (c) Mo/TiO_2, (d) Cr/TiO_2, and (e) Ag/TiO_2 nanocomposites in the 400- 4000 cm^{-1} wavenumber range are shown in **Figure. S2 (from the supporting information)**. All samples exhibited an absorption band in the 3800-3000 cm^{-1} range, which is attributed to the stretching vibrations of OH from physiosorbed water molecules. The contribution due to water proton absorption is represented by the absorption band around 1620 cm^{-1}. The strong band in the 900-450 cm^{-1} range is associated with Ti-O-Ti vibration in TiO_2 [37-38]. The small adsorption bands 2300 cm^{-1} in the Mo/TiO_2 and Ag/TiO_2 spectra correspond to atmospheric CO_2.

Catalytic activity

The Mars-Van Krevelen (MVK) mechanism has been widely used to describe the catalytic oxidation of VOCs over metallic oxides [39-40]. The mechanism consists of two independent steps: the oxidation of VOC molecules to CO_2 and H_2O via surface oxygen species and the reaction between reduced sites and oxygen from a gas phase to form surface oxygen species. Consequently, the surface oxygen species and the reducibility of the catalyst are critical for the overall oxidation of VOCs. **Figure. 3** illustrates the catalytic properties of TiO_2 and M/TiO_2 catalysts in HCHO oxidation. All catalysts, except TiO_2, were able to completely oxidize formaldehyde under the tested conditions. The highest catalytic activity was observed for Ag/TiO_2, which achieved complete HCHO conversion at a relatively low temperature of 95 °C.

At 245 °C, the Co/TiO_2 catalyst also achieved complete conversion of HCHO. The Mo/TiO_2 catalyst exhibited much lower activity, with total elimination of formaldehyde occurring at 317 °C. Similarly, Cr/TiO_2 was able to completely decompose formaldehyde, but at a higher temperature of 298 °C. To compare different materials in the field of catalysis, two key parameters are commonly studied: the T_{50} and T_{90} temperatures, which correspond to the temperatures at which 50% and 90% conversion, respectively, are achieved. The most desirable sample is one that achieves 50% or 90% conversion at the lowest possible temperatures. **Figure. 4** presents a summary histogram of the T_{50} (in black) and T_{90} (in red) values for the different materials. Notably, TiO_2 support exhibited a T_{50} of 207 °C, while the lowest T_{50} was observed for Ag/TiO_2, which achieved 50% conversion at 79 °C. The Co/TiO_2 and Mo/TiO_2 catalysts exhibited T50 values of around 143 °C and 232 °C, respectively, while Cr/TiO_2 had the highest T_{50} of 248 °C. It is worth mentioning that TiO_2 conversion did not exceed 85% for T_{90}, which is why **Figure. 3** does not display a T_{90} value for this sample. Nevertheless, the T_{90} values for all substituted materials were measured. The most active catalyst, with a T_{90} of 90 °C, was Ag/TiO_2, which achieved a lower T_{90} than the T_{50} values of the other modified materials. By contrast, the T_{90} values for Co/TiO_2, Cr/TiO_2, and Mo/TiO_2 were found to be 224 °C, 290 °C, and 309 °C, respectively.

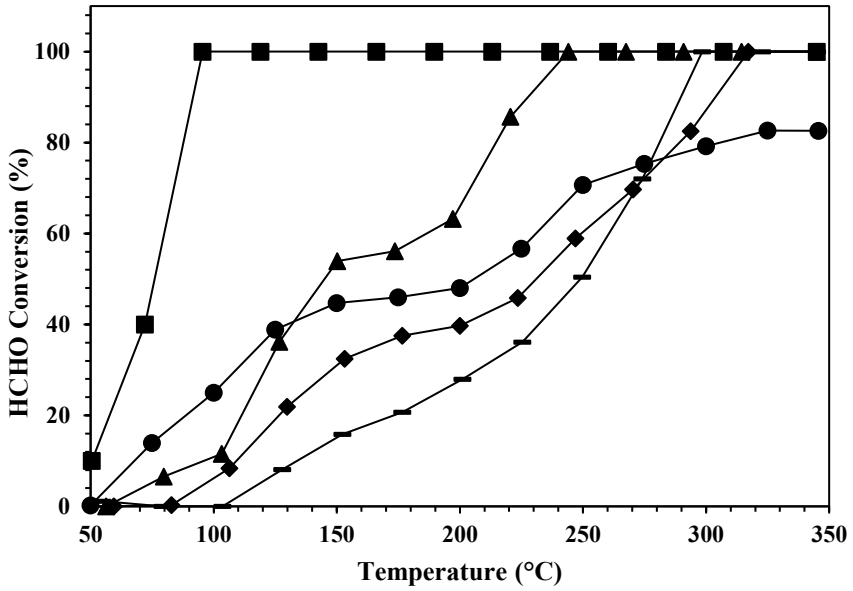

Figure. 3 HCHO conversions on: (●) TiO_2, (▲) Co/TiO_2, (—) Cr/TiO_2, (♦) Mo/TiO_2 and (■) Ag/TiO_2. Reaction conditions: HCHO 100 ppm, catalyst mass 50 mg, O_2 19.5 vol%, total flow rate 100 cm^3min^{-1}, GHSV 84000h^{-1}

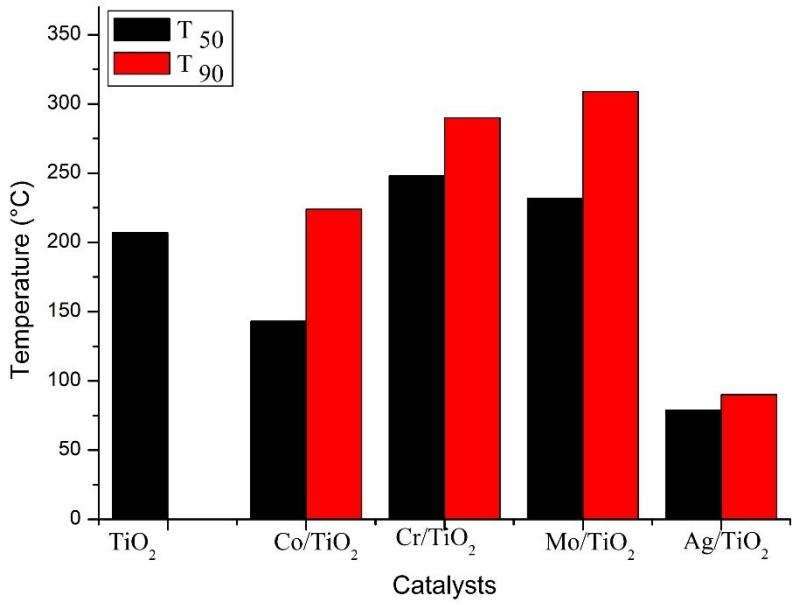

Figure. 4 Histogram of T_{50} and T_{90} in catalytic oxidation of formaldehyde according to the catalysts tested, HCHO 100 ppm, catalyst mass 50 mg, O_2 19.5 vol%, total flow rate 100 cm^3min^{-1}, GHSV 84000h^{-1}

The activity is not the only factor to consider when selecting a catalyst; selectivity is also important. Because the most active material is also the most selective in terms of harmful byproducts, it was unsuitable for indoor HCHO removal. As a result, it is necessary to compare the product yields obtained from various materials. Three products are detected under our experimental conditions: CO_2, CO, and CH_3OH, with the formic acid not being observed (**Figure. S3 from the supporting information**). At the temperature range of 50 to 350 °C, H_2O and CO_2 (**Fig. S3.a**) were the only products for the catalyst Ag/TiO_2, however, an important amount of CO (Fig. **S3.b**) was detected at over 200 °C produced by TiO_2 support, Cr/TiO_2, and Mo/TiO_2. As can be seen from **Fig. S3.c,** methanol could be detected when the reaction temperature was 52 °C for TiO_2, 60 °C for Co/TiO_2, 80 °C for Cr/TiO_2, and 100 °C for Mo/TiO_2. The yield of the different samples is in the following order:

$Ag/TiO_2 > Co/TiO_2 > Cr/TiO_2 > Mo/TiO_2 > TiO_2$.

This result shows that the redox sites created by silver species are more reactive in formaldehyde oxidation to CO_2 than the sites generated by molybdenum and chromium. The Co/TiO_2 sites have the potential to convert the HCHO and CH_3OH generated into CO_2 at 250

°C. Ag/TiO_2 can generate more active sites for HCHO oxidation than the other catalysts, and to compare with some literature data, **Table. 2** showed the activities of some of the different Ag-based catalysts.

Table 2. Catalytic activity of silver-based catalysts in the HCHO oxidation

Catalysts	Reactions conditions	T_{50} (°C)	References
Ag/TiO_2	100 ppm HCHO, O_2 19.5 vol%, GHSV 84000h^{-1}	79	This work
Ag/CeO_2	810 ppm HCHO, O_2 20 vol%, 84000 h^{-1} SV	90	[41]
Ag-HMO	400 ppm HCHO, 10 vol% O_2, 30.000 ml(gh) SV	80	[42]

With GHSV: gas hourly space velocity

Transmission electron microscopy

In order to better understand the variations in catalytic activity, the morphology and microstructure of the samples were analysed using transmission electron microscopy (TEM) techniques. **Figure. 5** provides representative TEM images of the calcined TiO_2 and M/TiO_2 samples. **Figure. 5a** displays the disordered but highly mesoporous structure of the TiO_2 support, which has a lattice spacing of 0.356 nm indexed as (101) and is identified as the anatase phase [43]. The Co/TiO_2 sample, depicted in **Figure. 5b**, exhibits well-defined spherical shapes with an agglomerated structure. **Figure. 5c** illustrates that the chrome catalyst only contains large metal particles within the size range of 30-200 nm, with no small Cr nanoparticles detected, and the Cr particles being larger than the other metal particles. As shown in **Figure. 5d**, the presence of Mo particles on the surface of the TiO_2 support is consistent with the particle size of 19.1 nm determined from X-ray diffraction (XRD) patterns using Scherrer's equation (as shown in Table 1). The Mo particles are too large to be located within the pores of the TiO_2. **Figure. 5e** shows that the distribution of Ag particles is relatively uniform. The addition of silver has resulted in some black spots with a hexagonal structure, indicating that Ag nanoparticles have been successfully loaded onto the surface of TiO_2. When combined with our XRD and BET analyses, it can be concluded that the surface area of the support favours the high dispersion of the metal. **Table. 3** displays the chemical composition of each sample analysed through EDS elemental analyses. The findings indicate that the chemical composition of each impregnated element is close to that theoretically estimated.

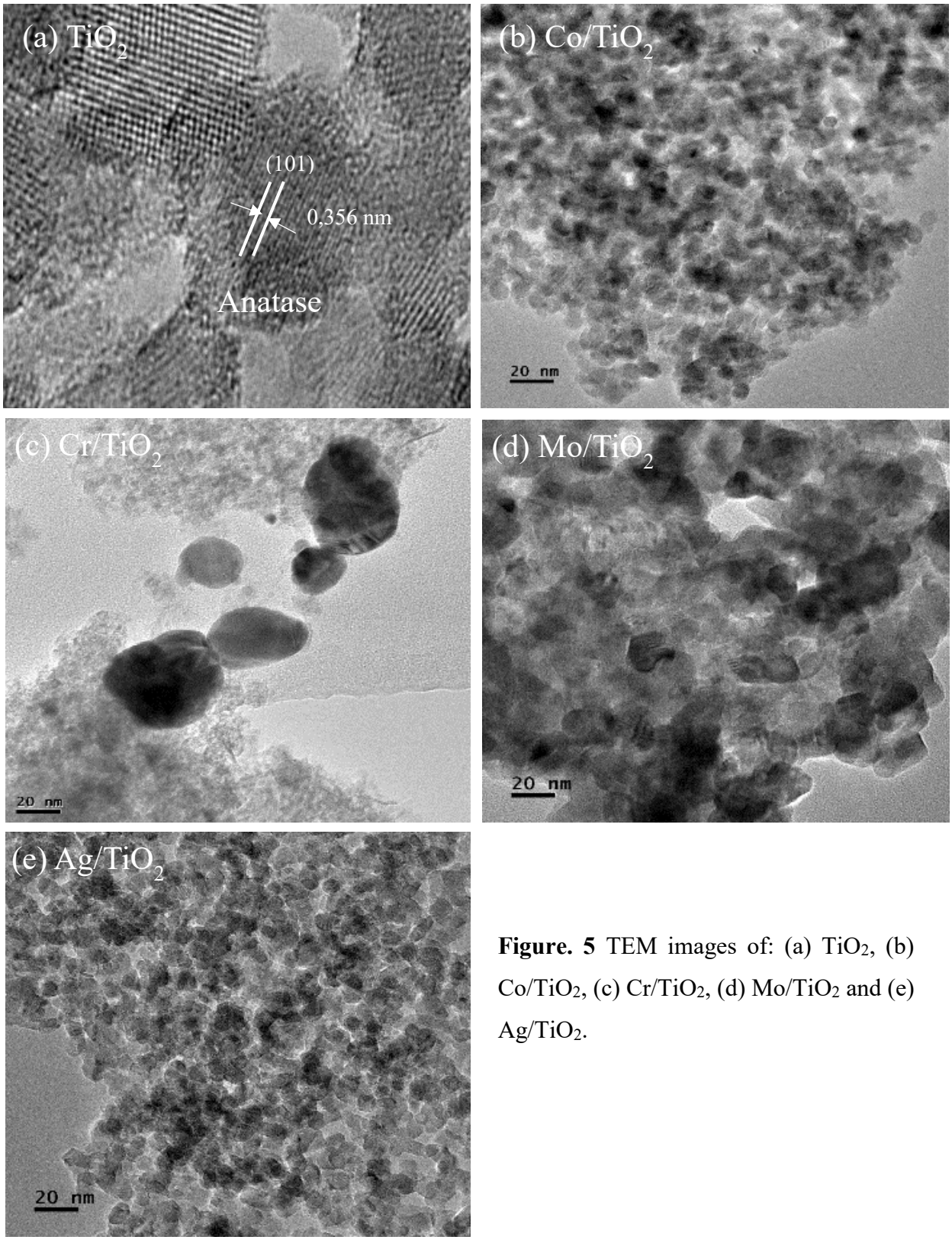

Figure. 5 TEM images of: (a) TiO_2, (b) Co/TiO_2, (c) Cr/TiO_2, (d) Mo/TiO_2 and (e) Ag/TiO_2.

Table. 3 EDS analysis of the different samples

Element	TiO_2 Wt%	5%Co/TiO_2 Wt%	5%Cr/TiO_2 Wt%	5%Mo/TiO_2 Wt%	5%Ag/TiO_2 Wt%
Ti	65.18	64.15	60.54	62.33	60.32
O	34.82	31.36	34.45	33.00	35.12
Co	-	4.49	-	-	-
Cr	-	-	5.01	-	-
Mo	-	-	-	4.67	-
Ag	-	-	-	-	4.56
Total	100.00	100.00	100.00	100.00	100.00

Conclusion

In summary, the addition of metals (Co, Cr, Mo, and Ag) to the TiO_2 support, prepared using sol-gel and impregnation methods, significantly affected the conversion of formaldehyde (HCHO). XRD analysis revealed the presence of the anatase phase of TiO_2 support, the existence of $CrCl_3$ in the Cr/TiO_2 catalyst, and metallic Mo in the solid Mo/TiO_2. BET analysis showed the similarity of the isotherms characterized by a mesoporous texture. TPR confirmed the existence of reduction peaks of silver and cobalt, which had an impact on the oxidative character of the catalysts.

The catalytic tests demonstrated that the Ag/TiO_2 catalysts exhibited superior catalytic activity, achieving 100% conversion of HCHO at 95°C and being the most selective for the production of CO_2. An improvement in catalytic activity was attributed to the presence of Co, which showed advanced activity for the complete oxidation of HCHO and selectivity for CO_2. The presence of Mo and Cr catalysts led to high production of carbon monoxide.

Conflict of interest

The authors declare no conflicts of interest

References

[1] Yang Y, Zhao S, Cui L, Bi F, Zhang Y, Liu N, Wang Y, Liu F, He C, Zhang X (2022) Recent advancement and future challenges of photothermal catalysis for VOCs elimination: From catalyst design to applications, Green Energy Environ. https://doi.org/10.1016/j.gee.2022.02.006

[2] Wang Y, Wang C, Zeng K, Wang S, Zhang H, Li X, Wang Z, Zhang C (2022) Revealing the strong interaction effect of MnO_x nanoparticles and Nb_2O_5 supports with variable morphologies on catalytic propane, Appl. Surf. Sci 576: 151797. https://doi.org/10.1016/j.apsusc.2021.151797

[3] Zhang X, Gao B, Creamer A.E, Cao C, Li Y (2017) Adsorption of VOCs onto engineered carbon materials, J. Hazardous Mater 338: 102-123 https://doi.org/10.1016/j.jhazmat.2017.05.013

[4] Costa S, Costa C, Madureira J, Valdiglesias V, Teixeira-Gomes A, Pinho P.G, Laffon B, Teixeira J.P (2019) Occupational exposure to formaldehyde and early biomarkers of cancer risk, immunotoxicity and susceptibility, Environ Res 179: 108740 https://doi.org/10.1016/j.envres.2019.108740

[5] Bai BY, Qiao Q, Li JH, Hao JM (2016) Progress in research on catalysts for catalytic oxidation of formaldehyde. Chin. J. Catal 37: 102-122. https://doi.org/10.1016/S1872-2067(15)61007-5

[6] Le Y, Guo DP, Cheng B, Yu JG (2013) Bio-template-assisted synthesis of hierarchically hollow SiO_2 microtubes and their enhanced formaldehyde adsorption performance. Appl. Surf. Sci 274: 110-116. https://doi.org/10.1016/j.apsusc.2013.02.123

[7] Arabzadeh A, Salimi A (2016) One dimensional CdS nanowire@TiO_2 nanoparticles core-shell as high performance photocatalyst for fast degradation of dye pollutants under visible and sunlight irradiation. J. Colloid. Interface. Sci 479: 43-54. https://doi.org/10.1016/j.jcis.2016.06.036

[8] Bai BY, Arandiyan H, Li JH (2013) Comparison of the performance for oxidation of formaldehyde on nano-Co_3O_4, 2D-Co_3O_4, and 3D-Co_3O_4 catalysts. Appl. Catal. B: Envi 142-143: 677-683. https://doi.org/10.1016/j.apcatb.2013.05.056

[9] Zhang C, He H, Tanaka KI (2006) Catalytic performance and mechanism of a Pt/TiO_2 catalyst for the oxidation of formaldehyde at room temperature. Applied Catalysis B Environmental, 65: 37-43. https://doi.org/10.1016/j.apcatb.2005.12.010

[10] Feng LL, Han X, Wang HB (2014) Preparation, characterization and catalytic formaldehyde oxidation at room temperature of MnO_X. Advanced Materials Research 873: 598-602. https://doi.org/10.4028/www.scientific.net/AMR.873.598

[11] Tang XF, Li YG, Chen JL, Huang XM, Xu YD, Shen WJ (2005) Manganese-Cerium Mixed Oxide Catalysts for Complete Oxidation of Formaldehyde: Effect of Preparation Method and Calcination Temperature. Applied Catalysis B Environmental 26: 265-273. https://doi.org/10.1016/j.apcatb.2005.08.004

[12] Ma C, Wang D, Xue W, Dou B, Wang H, Hao Z (2011) Investigation of formaldehyde oxidation over Co_3O_4-CeO_2 and Au/Co_3O_4-CeO_2 catalysts at room temperature: effective removal and determination of reaction mechanism, Environmental Science & Technology 45: 3628-3634. https://doi.org/10.1021/es104146v

[13] Xia Y, Dai H, Zhang L, Deng J, He H, Au CT (2010) Ultrasound-assisted nanocasting fabrication and excellent catalytic performance of three-dimensionally ordered mesoporous chromia for the combustion of formaldehyde, acetone, and methanol. Applied Catalysis B Environmental 100: 229-237. https://doi.org/10.1016/j.apcatb.2010.07.037

[14] Wang C, Liu H, Chen T, Qing C, Zou X, Xie J, Zhang X (2018) Synthesis of palygorskite-supported $Mn_{1-x}Ce_xO_2$ clusters and their performance in catalytic oxidation of formaldehyde, Applied Clay Science 159: 50-59. https://doi.org/10.1016/j.clay.2017.08.023

[15] Lochar V, FT-IR (2006) study of methanol, formaldehyde and methyl formate adsorption on the surface of Mo/Sn oxide catalyst, Applied Catalysis A: General 309: 33-36. https://doi.org/10.1016/j.apcata.2006.04.030

[16] Sekine Y (2002) Oxidative decomposition of formaldehyde by metal oxides at room temperature. Atmospheric Environment 36: 5543-5547. https://doi.org/10.1016/S1352-2310(02)00670-2

[17] Amin SA, Pazouk M, Hosseinnia A (2009) Synthesis of TiO_2–Ag nanocomposite with sol–gel method and investigation of its antibacterial activity against E. coli. Powder Technology 196: 241-245. https://doi.org/10.1016/j.powtec.2009.07.021

[18] Dimitriev Y, Ivanova Y, Iordanova R (2008) History of sol-gel science and technology. Journal of the University of Chemical Technology and Metallurgy 43: 181-192.

[19] Uncu O, Ozen B, & Tokatli F (2019) Use of FTIR and UV–visible spectroscopy in determination of chemical characteristics of olive oils. *Talanta*, *201*, 65–73. https://doi.org/10.1016/j.talanta.2019.03.116

[20] Fang R, He M, Huang H, Feng Q, Ji J, ZHAn Y, Leung DYC, Zhao W (2018) Effect of redox state of Ag on indoor formaldehyde degradation over Ag/TiO_2 catalyst at room temperature. Chemosphere 213: 235-243. https://doi.org/10.1016/j.chemosphere.2018.09.019

[21] Bhat A, Hill AJ, Fisher GB, Schwank JW (2021) Improving the thermal stability and n-butanol oxidation activity of Ag-TiO_2 catalysts by controlling the catalyst architecture and reaction conditions. Applied catalysis B: Environmental 297: 120476 https://doi.org/10.1016/j.apcatb.2021.120476

[22] Aazam E. S (2014) Visible light photocatalytic degradation of thiophene using Ag–TiO_2/multi-walled carbon nanotubes nanocomposite. Ceramics International, 40(5), 6705–6711. https://doi.org/10.1016/j.ceramint.2013.11.132

[23] Pirbazari A. E, Monazzam P, & Kisomi B. F (2017) Co/TiO_2 nanoparticles: preparation, characterization and its application for photocatalytic degradation of methylene blue. *DESALINATION AND WATER TREATMENT*, 283–292. https://doi.org/10.5004/dwt.2017.20205

[24] Ünlü B, & Özacar M (2020) Effect of Cu and Mn amounts doped to TiO_2 on the performance of DSSCs. *Solar Energy*, *196*, 448–456. https://doi.org/10.1016/j.solener.2019.12.043

[25] Thommes M, Kaneko K, Neimark AV, Olivier JP, Rodriguez-Reinoso F, Rouquerol J, Sing SW (2015) Physisorption of gases with special reference to the evaluation of surface area and pore size distribution. Pure ppl. Chem 87: 9-10. https://doi.org/10.1515/pac-2014-1117

[26] Yu J, Yu JC, Ho W, Leung MKP, Cheng B, Zhang G, Zhao X (2003) Effects of alcohol content and calcinations temperature on the textural properties of bimodally mesoporous titania. Appl. Catal. A-Gen. 255, 309-320. https://doi.org/10.1016/S0926-860X(03)00570-2

[27] Zhang T, Low J, Koh K, Yu J, Asefa T (2017) Mesoporous TiO_2 comprising small highly crystalline nanoparticles for efficient CO_2 reduction by H_2O. ACS Sustain. Chem. Eng. 6, 531-540. https://doi.org/10.1021/acssuschemeng.7b02827

[28] Zeng K, Li X, Wang C, Guo P, Yu J, Zhang C, Zhao X.S (2020) Three-dimensionally macroporus $MnZrO_x$ catalysts for propane combustion: Synergistic structure and doping effects on physicochemical and catalytic properties, J. Colloid Interface Sci 572: 281-296 https://doi.org/10.1016/j.jcis.2020.03.093

[29] Li S, Lin Y, Wang D, Zhang C, Wang Z, Li X (2021) Polhedral cobalt oxide supported Pt nanoparticles with enhanced performance for toluene catalytic oxidation, Chemosphere 263 : 127870 https://doi.org/10.1016/j.chemosphere.2020.127870

[30] Tran S.B.T, Choi H, Oh S, Park J.Y (2019) Defective Nb_2O_5-supported Pt catalysts for CO oxidation: Promoting catalytic activity via oxygen vacancy engineering, J. Catal 375: 124-134 https://doi.org/10.1016/j.jcat.2019.05.017

[31] Inturi S. N.R, Boningari T.h, Suidan M, Smirniotis P.G (2014) Visible-light-induced photodegradation of gas phase acetonitrile using aerosol-made transition metal (V, Cr, Fe, Co, Mn, Mo, Ni, Cu, Y, Ce, and Zr) doped TiO_2, Appl. Catal. B 144: 333-342. https://doi.org/10.1016/j.apcatb.2013.07.032

[32] Yang Y, Zhao S, Bi F, Chen J, Li Y, Cui L, Xu J, Zhang X (2022) Oxygen-vacancy-induced O_2 activation and electron-hole migration enhance photothermal catalytic toluene oxidation, Cell Reports Physical Science 33: 101011. https://doi.org/10.1016/j.xcrp.2022.101011

[33] Rahman A, Ahmed M (1995) Dehydrogenation of propane over chromia/alumina: A comparative characterization study of fresh and spent catalysts. Catalysts in Petroleum Refining

and Petroleum Refining and petrochemical Industries 100: 419-426. https://doi.org/10.1016/S0167-2991(96)80041-3

[34] Nilius N, Freund H-J (2015) Activating nonreducible oxides via doping. Acc Chem Res 48(5):1532–1539. https://doi.org/10.1021/acs.accounts.5b00018

[35] Wang Y, Bi F, Wang Y, Jia M, Tao X, Jin Y, Zhang X (2021) MOF-derived CeO_2 supported Ag catalysts for toluene oxidation: The effect of synthesis method. J. Molecular catalysis 515: 111922. https://doi.org/10.1016/j.mcat.2021.111922

[36] Chernykh M, Mikheeva N, Zaikovskii V, Salaev M, Liotta L. F, & Mamontov G (2020) Room-Temperature Nitrophenol Reduction over Ag–CeO_2 Catalysts: The Role of Catalyst Preparation Method. *Catalysts*, *10*(5), 580. https://doi.org/10.3390/catal10050580

[37] Yu J, Su Y, Cheng B, Zhou M (2006) Effects of pH on the microstructures and photocatalytic activity of mesoporous nanocrystalline titania powders prepared via hydrothermal method. Journal of Molecular Catalysis A: Chemical 258(1-2):104-112. https://doi.org/10.1016/j.molcata.2006.05.036

[38] Sakthivel T, kumar KA, Ramanathan R, Senthilselvan J, Jagannathan K (2017) Silver doped TiO_2 nano crystallites for dye-sensitized solar cell (DSSC) applications. Materials Research Express 4. https://doi.org/10.1088/2053-1591/aa9e36

[39] Pei J, Zhang JS (2011) Critical review of catalytic oxidization and chemisorption methods for indoor formaldehyde removal. HVAC&R Res 17: 476-503. Doi 10.1080/10789669.2011.587587

[40] Popova M, Szegedi Á, Cherkezova-Zheleva Z, Dimitrova A, Mitov I (2010) Toluene oxidation on chromium-and copper-modified SiO_2 and SBA-15. Applied Catalysis A: General 381: 26-35. https://doi.org/10.1016/j.apcata.2010.03.040

[41] Ma L, Wang D, Li J, Bai B, Fu L, Li Y (2014) Ag/CeO_2 nanospheres: Efficient catalysts for formaldehyde oxidation. Applied catalysis B: Environmental 148-149: 36-43. https://doi.org/10.1016/j.apcatb.2013.10.039

[42] Huang Z, Gu X, Cao Q, Hu P, Hao J, Li J, Tang X (2012) Catalytically Active Single-Atom Sites Fabricated from Silver Particles. Angew. Chem. Int. Ed 124: 4274-4279. https://doi.org/10.1002/ange.201109065

[43] Dai S, Wu Y, Sakai T, Du Z, Sakai H, Abe M (2010) Preparation of Highly Crystalline TiO_2 Nanostructures by Acid-assisted Hydrothermal Treatment of Hexagonal-structured Nanocrystalline Titania/Cetyltrimethyammonium Bromide Nanoskeleton. Nanoscale Res Lett 5: 1829-1835. DOI 10.1007/s11671-010-9720-0